HHS Public Access

Author manuscript

J Therm Biol. Author manuscript; available in PMC 2021 July 01.

Published in final edited form as:

J Therm Biol. 2020 July ; 91: 102644. doi:10.1016/j.jtherbio.2020.102644.

A Review on Numerical Modeling for Magnetic Nanoparticle Hyperthermia: Progress and Challenges

Izaz Raouf[a], **Salman Khalid**[a], **Asif Khan**[a], **Jaehun Lee**[a,*], **Heung Soo Kim**[a,*], **Min-Ho Kim**[b,*]

[a]Department of Mechanical, Robotics and Energy Engineering, Dongguk University-Seoul, 30 Pildong-ro 1-gil, Jung-gu, Seoul 100-715, Republic of Korea

[b]Department of Biological Sciences, Kent State University, Kent, OH 44242, USA

Abstract

Recent progress in nanotechnology has advanced the development of magnetic nanoparticle (MNP) hyperthermia as a potential therapeutic platform for treating diseases. Due to the challenges in reliably predicting the spatiotemporal distribution of temperature in the living tissue during the therapy of MNP hyperthermia, critical for ensuring the safety as well as efficacy of the therapy, the development of effective and reliable numerical models is warranted. This article provides a comprehensive review on the various mathematical methods for determining specific loss power (SLP), a parameter used to quantify the heat generation capability of MNPs, as well as bio-heat models for predicting heat transfer phenomena and temperature distribution in living tissue upon the application of MNP hyperthermia. This article also discusses potential applications of the bio-heat models of MNP hyperthermia for therapeutic purposes, particularly for cancer treatment, along with their limitations that could be overcome.

Graphical Abstract

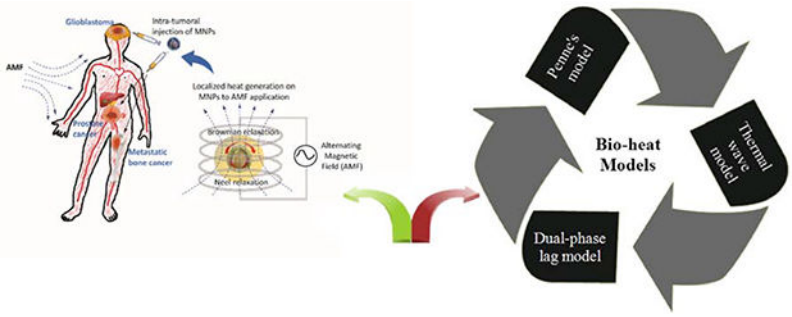

*Corresponding authors: jaehun@dgu.edu, heungsoo@dgu.edu; Tel: +82-2-2260-8577, Fax: +82-2-2263-9379 mkim15@kent.edu; Tel: 1-330-672-1445.

Keywords

Cancer Treatment; Magnetic Fluid Hyperthermia; Induction Heating; Specific Loss Power; Bio-heat Modeling; Heat Transfer Analysis

1. Introduction

Recent progress in nanotechnology has advanced the development of magnetic nanoparticle (MNP) hyperthermia platform for various biomedical applications, especially for therapeutic purposes (Johannsen et al., 2010). Hyperthermia is a treatment method which induces cellular apoptosis and death by increasing tissue temperature. Depending on the magnitude of the temperature and exposure time, hyperthermia is divided into three categories including, long-term low temperature hyperthermia, moderate temperature hyperthermia, and thermal ablation or high temperature hyperthermia (Habash et al., 2006) (Fig. 1). Although hyperthermia therapy has been widely conducted through preclinical studies and clinical trials, its translation into clinics has been limited by the lack of specificity against target cells, which causes non-specific thermal toxicity to the healthy host tissue. The principle of MNP hyperthermia is to achieve a localized increase in temperature in target cells by the localized activation of MNPs upon exposure to a high frequency alternating magnetic field (AMF). Gilchrist *et al.* (Gilchrist et al., 1957) introduced MNP hyperthermia for the first time as a means to kill lymphatic metastases in dogs. Since then, numerous studies of applying MNP hyperthermia have been conducted as a new therapeutic platform that could overcome the limitation of conventional hyperthermia therapy. In particular, numerous cellular and pre-clinical studies demonstrated its therapeutic potential for the treatment of cancer diseases (Chang et al., 2018; Liu et al., 2020). Additionally, MNP hyperthermia has emerged as a promising strategy for the treatment of bacterial infections (Alumutairi et al., 2020; Kim et al., 2013).

Recent clinical trials for MNP hyperthermia have demonstrated its safety and therapeutic feasibility as an anti-cancer therapy for patients with glioblastoma, prostate cancer, and metastatic bone cancer (Fig. 2). The first clinical feasibility study on MNP hyperthermia was conducted in 2003 with 14 patients with glioblastoma multiforme (Maier-Hauff et al., 2007). This study showed that the application of MNP hyperthermia could generate desired temperatures in the tumor, ranging between 42.4°C to 49.5°C. A subsequent study from the group determined that MNPs could be safely used in the treatment of patients suffering with recurrent glioblastoma multiforme (Maier-Hauff et al., 2011). Johannsen et al. (Johannsen et al., 2007) conducted the phase I clinical study of MNP hyperthermia from 10 patients with local recurrence of prostate cancer and evaluated the feasibility of the therapy. The decrease in prostate-specific antigen (PSA) was observed from eight patients after treatment, demonstrating the feasibility of MNP hyperthermia for the treatment of local recurrence of prostate cancer without eliciting significant side effects. Wust et al. (Wust et al., 2006) conducted MNP hyperthermia treatment for 22 patients with relapsed tumor entities to evaluate the feasibility of the technology. Matsumine et al. (Matsumine et al., 2007) used calcium phosphate bone cement containing iron oxide MNPs for treatment of patients with

metastatic bone tumors. The group of patients with postoperative MNP hyperthermia showed a better efficacy than the group with surgery alone.

The effectiveness of MNP hyperthermia therapy is highly dependent on the temperature rise achieved during the treatment. The exposure of AMF to MNPs causes the conversion of electromagnetic energy into heat energy via mechanisms such as Brownian relaxation, Neel relaxation and Hysteresis losses (Sasayama et al., 2015). The heat generation on MNPs to the exposure of AMF is quantified by specific loss power (SLP), also referred to as specific absorption rate (SAR), a parameter used to quantify the efficiency of MNPs in converting electromagnetic energy into heat (Arora et al., 2002). Various empirical methods are used to evaluate the SLP from an experimental setup, such as the initial slope, corrected slope, Box-Lucas and steady state methods (Bordelon et al., 2011; Natividad et al., 2008). Besides, the SLP value can be determined analytically using methods such as the linear response theory (LTR) (Carrey et al., 2011), the Rayleigh model (Dutz and Hergt, 2014) and the Stoner-Wohlfarth model (Thirion et al., 2002). The effectiveness of heat generation by MNPs is significantly influenced by various parameters, such as the material type (Wadehra et al., 2017), size (Bakoglidis et al., 2012), concentration (Bellizzi et al., 2016) and spatial distribution of MNP (Golneshan and Lahonian, 2011), anisotropy of MNP structure (Carrey et al., 2011), viscosity of the supporting medium (Kalambur et al., 2005), and the strength and frequency of AMF (Shubitidze et al., 2015).

Having the ability to control the heat distribution in living tissues is critical for the clinical applications of MNP hyperthermia. Although the extent of heat dissipation from MNPs can be tuned by controlling the parameters mentioned above, it is quite challenging to predict temperature distribution in living tissue due to various factors, such as complicated geometry, heat conduction in tissues, blood perfusion and metabolic heat generation. In this regard, various bio-heat models for predicting heat transfer phenomena and temperature distribution in living tissue have been developed. Among the widely used bio-heat transfer models are: Pennes' bio-heat transfer model (PBHTM), the thermal wave bio-heat transfer model (TWBHTM) and the dual-phase lag bio-heat transfer model (DPLBHTM). The PBHTM is the first bio-heat model developed to predict temperature distribution in living tissues (Pennes, 1948). The TWBHTM and DPLBHTM were proposed to further improve the prediction of tissue temperature distribution by incorporating the effect of a single-phase lagging (Cattaneo, 1958) and double-phase lagging (Tzou, 1997) of heat wave propagation, respectively, which might occur due to the thermal relaxation associated with a non-Fourier thermal behavior of biological tissues.

This review paper attempts to provide a comprehensive understanding on the analytical and numerical modeling of MNP hyperthermia for predicting temporal and spatial distribution of temperature in the biological tissues. To address this, first, different heating mechanisms of MNP hyperthermia, along with parameters affecting the extent of heat generation from MNPs, are explained in the context of analytical and empirical models for SLP calculations. Second, different bio-heat models for predicting thermal behavior of biological tissue are introduced. Lastly, biomedical applications of the bio-heat models for predicting temperature distribution in living tissue during MNP hyperthermia, particularly for cancer treatments, are discussed, along with its opportunities and challenges.

2. Heating Mechanisms of MNP Hyperthermia

The applied AMF can exhibit heating effects in the magnetic material by triggering eddy currents, hysteresis losses, or relaxations such as Brownian and Neel relaxations (Deatsch and Evans, 2014). The eddy current is dominant in materials having the size of centimeters or higher. It produces resistive heating due to the rapid change in the alternating magnetic flux. On the other hand, heat generation from MNPs upon exposure to AMF is mediated by either hysteresis losses, Brownian relaxation, or Neel relaxation, depending on the frequency of AMF and size of MNP, associated with the alteration of the domain wall in multi-domain magnetic materials (Dennis and Ivkov, 2013). Heat generation by hysteresis losses can occur in large MNPs with multiple magnetic domains, where the orientation of the magnetic moments tends to align continuously with the direction of the magnetic field (Chang et al., 2018). In general, Brownian and Neel relaxations have been considered to be the dominant mechanism that elicits heating effects in MNPs for single domain superparamagnetic nanoparticles. The magnetic motion is fixed along with the pivot of rotation in the Brownian relaxation, and the particles start rotation against a supporting medium when the field direction aligns the magnetic moment, which triggers a frictional force that generates heat. In Neel relaxation, the magnetic moment rotates inside the magnetic particle against particle's crystalline structure, resulting in heat generation. Neel and Brownian relaxations are characterized by their relaxation time as given in the following equations (Rosensweig, 2002);

$$\tau_B = \frac{3\eta V_h}{k_B T} \tag{1}$$

$$\tau_N = \frac{\sqrt{\pi}}{2}\tau_0 \frac{\exp\Gamma}{\Gamma^{3/2}} \tag{2}$$

$$\tau = \frac{\tau_B \tau_N}{\tau_B + \tau_N} \tag{3}$$

Where τ_B, τ_N, τ_0 and denote the Brownian relaxation time, Neel relaxation time, time constant, and effective relaxation time, respectively. η, k_B, T, and V_h denote the viscosity of the fluid, Boltzmann constant, absolute temperature, and hydrodynamics volume of the nanoparticle, respectively.

The term Γ can be further defined as;

$$\Gamma = \frac{kV_m}{k_B T} \tag{4}$$

Where k is the anisotropy constant and V_m is the geometric volume of the nanoparticle. The hydrodynamic volume of nanoparticle is related to the geometric volume as follow;

$$V_h = (1 + \delta/R)^3 V_m \tag{5}$$

where δ is the surfactant layer thickness (Miaskowski and Sawicki, 2013). These expressions show that the Brownian relaxation is a function of the hydrodynamic volume of the MNPs and viscosity of the fluid. The Neel relaxation is strongly dependent on the size of the nanoparticles. In general, smaller sized nanoparticles are preferable than larger ones for hyperthermia purposes since they require less power for inducing a magnetic moment and exhibit low resistance of particle rotation under high viscosity of media (Lévy et al., 2008).

2.1. Analytical models for calculating SLP

The reliable estimation of SLP for the given MNPs is critical to assess the heating efficiency of MNP hyperthermia. In view of this, various analytical methods for calculating SLP have been proposed by introducing a dimensionless parameter of magnetic-thermal quantity (ξ) (Carrey et al., 2011) as;

$$\xi = \frac{\mu_0 M_s V H_{\max}}{k_B T} \tag{6}$$

where μ_0, M_s, and $H_{\max}$ denote the permeability of free space, saturation of magnetization, and maximum applied field, respectively. If ξ<<1, the LRT can be applied for calculating SLP, where the direct relationship between SLP and AMF strength is represented as $SLP \propto H^2$. The LRT could be applied for a single-domain, superparamagnetic region (Fig. 3). However, if ξ>1, the Rayleigh model must be used for SLP calculation, where $SLP \propto H^2$ (Dutz and Hergt, 2014). Although the Rayleigh model has been proposed for ferromagnetic (multi-domain state) materials, it can also be applied for single domain state materials in the case of the coherent reversal. The Stoner-Wohlfarth model (SWM) is applicable for a ferromagnetic or blocked domain if the condition of $\mu_0 H_{\max} > 2\mu_0 H_c$ is satisfied, where H_c is the coercive field of MNPs. Although H_c is a function of the size of MNPs, there are ferromagnetic regions where the LRT could still be applied (Kasyutich et al., 2010; Lyutyy et al., 2015).

The generalized form of heat dissipation (P) equation can be represented as (Bekovic and Hamler, 2010);

$$P = \pi \mu_0 \chi_0 H^n f \frac{2\pi f \tau}{1 + (2\pi f \tau)^2} \tag{7}$$

Where μ_0 is the permeability of free space, χ_0 is the static equilibrium susceptibility, and f is the frequency of AMF. The static equilibrium susceptibility can be further given as:

$$\chi_0 = \chi_i \frac{3}{\xi}\left(\mathrm{Coth}\xi - \frac{1}{\xi}\right) \tag{8}$$

where χ_i is initial susceptibility, which is given as;

$$\chi_i = \frac{\mu_0 \phi M_d^2 V_m}{3 K_B T} \tag{9}$$

Where ϕ is the volume fraction of MNPs, which correlates domain magnetization (M_d) with saturation magnetization ($M_s = \phi M_d$). The SLP can be represented in the form of heat dissipation as (Beković et al., 2019);

$$SLP = \frac{P}{\rho} \tag{10}$$

where ρ represent the density of particle in the fluid.

2.2. Empirical methods for measuring SLP

The SLP can be determined empirically by calorimetric heating measurements. For this, temperature changes in a fluid containing dispersed MNPs are measured over time during the application of AMF at a given field frequency and strength. Then, the measured temperature values are used to calculate SLP by using methods such as the initial slope method, corrected slope method, Box-Lucas method, and the steady state method.

Initial Slope Method—The initial slope method is the commonly used one in empirically measuring SLP due to its simplicity in calculation. The SLP value by initial slope method is calculated as (Andreu and Natividad, 2013);

$$SLP_{initial-slope} = C_{MF}\frac{\Delta T}{\Delta t}\frac{m_{MF}}{m_{MNPs}} \tag{11}$$

Where C_{MF} is the specific heat capacity of the magnetic fluid, m_{MF} is the mass of ferro-fluid, m_{MNPs} is the mass of the MNPs dispersed in a fluid, and $\frac{\Delta T}{\Delta t}$ is the initial slope in the temperature and time curve. Different time intervals can be taken to measure the initial slope of the heating curves, such as linear fit for the first ten seconds (Natividad et al., 2008) or time interval between 10 and 100 seconds (Wang et al., 2013). Additionally, numerical derivatives of the entire curve (Bordelon et al., 2011) or maximum slope (Teran et al., 2012) can be used to determine the initial slope.

Corrected Slope Method—This method was presented by Wildebore *et al.* (Wildeboer et al., 2014) to correct an error that might occur from any linear loss at the specific value of ΔT in using an initial slope method and can be expressed as;

$$SLP_{Corrected-slope} = \left(C\frac{dT}{dt} + L\Delta T\right)m_{MF}/m_{MNP} \tag{12}$$

Where ΔT is the temperature difference between the ferro-fluid and baseline, and L is the linear loss parameter and is calculated by determining the value that results in the smallest standard deviation between SLP values on the same heating curve (Lanier et al., 2019).

Box-Lucas Method—This method is based on non-linear experimental models in measuring ΔT, in which heating curves are fitted using an exponential equation (Sanz et al., 2015). The SLP value is calculated using the fitting parameters as follows (Bordelon et al., 2011);

$$SLP_{Box-Lucas} = (A\lambda C)m_{MF}/m_{MNP} \quad (13)$$

where A and λ are the fitting parameters that can be found from the experimental data, and their product can be calculated as;

$$A\lambda = T_{ss}\tau^{-1} \quad (14)$$

where T_{ss} represents the steady state temperature, and τ is the characteristic time of the system during the cooling process ($\tau = C/L$).

Steady state method—In this method, SLP is calculated using the temperature measured at the steady state condition in the heating curve as follows (Wildeboer et al., 2014);

$$SLP_{Steady-state} = (T_{ss}L)m_{MF}/m_{MNP} \quad (15)$$

2.3. Parameters influencing the heating efficacy of MNPs

The extent of heat dissipation from MNPs can be substantially influenced by various parameters of MNP and AMF, which include the material type, size, and concentration of MNPs, their spatial distribution and interactions within living tissue, and the strength and frequency of AMF. In fact, temperature profiles in living tissue during the treatment of MNP hyperthermia depend on the combined effects of these parameters. This section briefly summarizes published studies about the effects of the parameters on the efficacy of heat dissipation from MNPs (Table 1).

Materials for MNP—Iron oxide nanoparticles, particularly magnetite (Fe_3O_4) or maghemite (γ-Fe_2O_3) with sizes ranging from 10 to 100 nm, have been widely used as material for MNP hyperthermia due to its biocompatibility, capability of heat generation, and tunable properties (Abenojar et al., 2016; Chang et al., 2018). In addition to the use of iron oxide MNPs, numerous studies have been performed to improve the heating efficacy of MNPs by developing nanocomposite by means of mixing iron oxide particles with metallic magnetic particles such as cobalt. For example, cobalt-iron oxide MNPs were shown to exhibit an improved heat dissipation capacity compared to the control MNPs at a similar size (Habib et al., 2008), due to their larger saturation magnetization. Alternatively, low Curie temperature (LCT) material can be used to tune the extent of heat generation from MNPs. Tang *et al.* (Tang et al., 2017) showed that MNPs with LCT coating could exhibit better results than iron oxide MNPs.

Particle size—Since the extent of heat generation from MNPs made of the same material and composition is influenced by the size of particles, it is important to determine the optimal size of MNPs that could achieve a maximal heating effect. Numerous studies observed that iron oxide MNPs ranging from 10 nm (Bakoglidis et al., 2012), 11.2 nm (Engelmann et al., 2019), 12 nm (Purushotham and Ramanujan, 2010), 16 nm (Purushotham and Ramanujan, 2010), to 19 nm (Guardia et al., 2012), could exhibit an effective heating on MNPs. In line with this, the optimal size of nanoparticles for a maximum heating efficiency

was determined to be around 15 nm, which was associated with the balance between Brownian and Neel relaxations losses (Lévy et al., 2008). However, it should be noted that the determination for optimal size of MNPs can be influenced by experimental conditions such as the strength and frequency of applied AMF. For example, for power loss due to Néel relaxation, the optimum size of MNP was observed to be inversely proportional to increasing field frequency (Hergt et al., 1998). On the other hand, the optimal size of MNP appears to increase with increasing field strength. For example, in the study by Li *et al.* (Li et al., 2011), the optimal particle size was measured to be 8 nm at field strength of 9.6 kA/m and at frequency of 100 kHz. However, the heating efficiency of the same particles was measured to be best for larger size of MNP (~ 24 nm) when AMF was applied at field strength of 23 kA/m at the same frequency.

Anisotropy of MNP—The varying degree of anisotropy in MNPs has been shown to affect the heating efficacy of MNPs under AMF, which can be altered by synthesis method, shape, and surface coating. The anisotropy in MNPs is resulted from changes in atomic symmetry at the particle surface or magnetic dipole-dipole interactions due to particle agglomeration (Moreno et al., 2020). The maximum heating rate was shown to decrease with increasing the anisotropy of MNP at a given particle size (Habib et al., 2008). Carrey *et al.* (Carrey et al., 2011) proposed an analytical model that could be used to approximate the ideal anisotropy of MNP for generating an optimum heating by determining SLP values as a function of MNP anisotropy.

Viscosity of a supporting medium—The medium in which MNPs are dispersed also can affect the heating efficacy of MNPs. For the same type of MNP material, MNP dose, and AMF condition, higher SLP values were observed from MNPs dispersed in water than in glycerol (Kalambur et al., 2005). This effect appears to be due to the higher viscosity of collagen in glycerol, which might attenuate the capacity of MNPs to relax and dissipate heat by decreasing the probable collisions among MNPs. As such, in biological tissues, the heat loss by Brownian relaxation can be less effective due to the higher viscosity that might arise from the presence of extracellular matrix such as collagen in the tissue. The similar phenomenon was observed in the cellular environment as well (Di Corato et al., 2014), in which the measured SLP value was decreased by half associated with attenuation of the Brownian relaxation in cellular conditions.

The strength and frequency of AMF—The magnetic field strength and field frequency are the critical parameters that directly affect the efficacy of MNP hyperthermia by altering the extent of heat dissipation from MNPs. In general, the heat generation of MNPs increases with applied field strength (H) and field frequency (f). However, it is important to tune the level of applied field strength and frequency in order to avoid the generation of eddy current, which is proportional to the product of both quantities and can trigger a non-specific heating effect on healthy tissues (Nieskoski and Trembly, 2014). The clinical trials of MNP hyperthermia revealed that acceptable ranges of the product of H and f that are safe to the human patients were between 5×10^8 A/m·s and 8.5×10^8 A/m·s (Johannsen et al., 2007; Maier-Hauff et al., 2007). Cervadoro et al. (Cervadoro et al., 2013) systemically examined the effects of frequency (0.2 and 30 MHz) and field strength (4 to 10 kA/m) on the change in

temperature and SLP of superparamagnetic iron oxide nanoparticles. The non-specific heating was dominated at high frequency field (~30 MHz), which became negligible at low frequency field (<1 MHz). They showed that SLP of the MNPs varied linearly with f and H^2. In general, the safe range of AMF strength and frequency to avoid any non-specific heating effect by eddy current were shown to be between 0 to 15 kA/m and 0.05 to 1.2 MHz, respectively (Rast and Harrison, 2010).

Concentrations and distribution of MNPs—The amount of heat generated during the MNP hyperthermia is highly dependent on the concentration of MNPs dispersed in a medium or tissue. However, this effect should be assessed by considering cellular and tissue environments such as the size and type of supporting tissue as well. In the clinical trial of MNP hyperthermia for patients with recurrent glioblastoma, up to 31 mg of MNPs per cm^3 of tumor volume was injected intratumorally (Maier-Hauff et al., 2011). In a numerical study, Bellizzi *et al.*(Bellizzi et al., 2016) estimated an optimal concentration of MNP for a brain tumor by using the Zubal numerical model, which revealed that the concentration of MNPs up to 10 mg/mL could be sufficient for heating of brain tumors smaller than 10 mm. Besides, the degree of MNP mobilization resulted from the interaction between MNPs and surrounding tissue can also influence the extent of heat dissipation from MNPs. The immobilized state of MNPs within the tumor volume was associated with decrease in heat dissipation by 30%, compared to the condition with mobilized MNPs (Miaskowski and Subramanian, 2019). This suggests that it is important to consider whether MNPs are free to move or whether they are immobilized in the tissue in planning the concentration of MNPs for hyperthermia therapy.

On the other hand, the pattern that MNPs are dispersed in the tissue is another important parameter that influences temperature distribution profiles within living tissue. Gonneshan and Lahonian (Golneshan and Lahonian, 2011) investigated the effect of MNP dispersion on temperature elevation in a spherical shape of tumor using a bio-heat model involving the three-dimensional lattice Boltzmann method (LBM). They demonstrated that the MNPs dispersed by Gaussian distribution was more effective in heat dissipation for the spherical shape of tissue than homogenously dispersed MNPs. Additionally, the clustering of nanoparticles, commonly observed in biological tissue including a tumor tissue (Giustini et al., 2009), decreases the cluster domain magnetization and the average magnetic moment, resulting in the attenuation of heating efficiency and SLP values (Wang et al., 2017).

Blood perfusion—Blood perfusion plays an important role in redistribution of thermal energy in living tissue by acting as a major source of heat removal under hyperthermia (Lagendijk et al., 1988). Using a numerical model of spherical tissue with blood perfusion, Lahonian and Golneshan (Lahonian and Golneshan, 2011) showed that temperature in the tissue decreased with increase of blood flow rate. Lagendijk (Lagendijk, 1982) predicted temperature distribution by proposing a tissue model with a large blood vessel in the heated region based on the basic discrete vessel models. Numerical studies using more advanced three-dimensional models with branching vessel networks have also been proposed (Brinck and Werner, 1995, 1994). Using a three-dimensional tissue model embedded with a countercurrent blood vessel network, Huang et al. (Huang et al., 2010) demonstrated that a

region with vasculature could sustain more heat deposited than one without vasculature due to the cooling effect of blood vessels. These models provided more insight into the heat transfer process between blood and tissue compartments during hyperthermia and demonstrated the importance of incorporating the effect of blood vessels in the thermal behavior of living tissue.

Metabolic heat generation—Metabolic heat generation also affects the heat transfer in living tissues, which behaves like a heat generation source within the living organism and cannot be ignored for effective modeling of MNP hyperthermia (Lahonian and Golneshan, 2011). It has been reported that the metabolic heat generated per unit volume varies from organ to organ in the body (Wang et al., 2011). Lin and Liu (Lin and Liu, 2009) presented a numerical model of a bi-layered spherical tumor by considering the effect of metabolism in heat generation in the analysis domain. In addition, other studies have highlighted the importance of considering metabolism in their numerical modeling to reliably predict heat transfer phenomena during hyperthermia (Majee and Shit, 2017; Reis et al., 2016; Wang et al., 2012).

3. Bio-heat Models for MNP Hyperthermia

In order to achieve desired thermal toxicity against target cells, while avoiding non-specific thermal damage to the surrounding healthy tissue, it is critical to reliably predict temperature profiles in the affected living tissue. As discussed above, temperature distribution in living tissue during the treatment of MNP hyperthermia is influenced by not only the parameters of MNP and AMF, but also the tissue properties and characteristics associated with blood perfusion and tissue metabolism. In this regard, various bio-heat models have been developed as an effective tool that helps us optimize those parameters responsible for heat generation in living tissue as well as understand the mechanism underlying the hyperthermia treatment.

Since the application of MNP hyperthermia for therapeutic purposes has been largely developed for cancer therapy, most bio-heat models have been applied to predict temperature distribution in tumor tissue models. A geometrical domain for thermal modeling of MNP hyperthermia in a tumor tissue surrounded by vascular system and healthy tissue is depicted in Fig. 4. Among the models developed so far, three bio-heat models have been widely used, which include Pennes's bio-heat transfer model (PBHTM) (Pennes, 1948), thermal wave bio-heat transfer model (TWBHTM) (Cattaneo, 1958), and dual-phase lag bio-heat transfer model (DPLBHTM) (Tzou, 1997). Table 2 compares and summarizes the advantages and limitations of these bio-heat models.

3.1. Penne's Bio-heat transfer Model (PBHTM)

The PBHTM is the first kind of bio-heat model based on Pennes' bio-heat transfer equation with an aim of predicting the thermal behavior of living tissue by considering the effects of metabolism and blood perfusion on the thermal energy balance (Pennes, 1948). The equation for this model enables the inclusion of the effect of blood perfusion and metabolic heat generation by introducing factors that describe the heat exchange between blood vessels and tissue, in which it is assumed that metabolic heat generation and blood perfusion effects are

homogeneously distributed throughout the tissue. The generalized form of Pennes' bio-equation is given as (Arkin et al., 1994);

$$\rho c\frac{\partial T}{\partial t} = \nabla(k\nabla T) + w_b c_b(T_a - T) + q_m \tag{16}$$

Where ρ, c_b, and k represents density (kg/m^3), the specific heat capacity of the blood (J/kg/K), and thermal conductivity, respectively. w_b and q_m represent the flow rate of the blood per unit volume of tissue (kg/s.m^3) and the metabolic heat generation per unit volume of the tissue (W/m^3), respectively. T_a is the temperature of arterial blood (K); T is the temperature at the tissue at any particular instant; $\frac{\partial T}{\partial t}$ is the temperature gradient. The equation describes that the blood enters tissue volume at an arterial temperature and reaches equilibrium state at the tissue temperature. In order to include the effect of heat dissipation from MNPs, the equation is further modified as (Tang et al., 2018);

$$\rho_1 c_1\frac{\partial T}{\partial t} = \nabla(k_1\nabla T) + w_{b1} c_{b1}(T_a - T_1) + q_m + P_h \tag{17}$$

where P_h indicates the heat dissipated by MNPs in the tissue. The physical and thermal properties for the combined system of tissues and MNPs can be given by equations 18, 19 and 20;

$$\rho_1 = (1-\eta)\rho_r + \eta\rho_{MNP} \tag{18}$$

$$c_1 = (1-\eta)c_T + \eta c_{MNP} \tag{19}$$

$$1/k_1 = (1-\eta)/k_T + \eta/k_{MNP} \tag{20}$$

where the subscripts *T, MNP,* and η represent the tumor properties prior to the administration of MNPs, the properties of MNPs administered, and the volume fraction of MNPs in the tissue, respectively.

Numerous studies have applied the PBHTM model to predict the thermal behavior of biological tissues. Shih *et al.* (Shih et al., 2007) analyzed the thermal response of semi-infinite biological tissue due to a sinusoidal heat flux at the skin by solving the PBHTM by using the Laplace transform. Their analysis was suitable for describing the transient temperature response of tissue for the whole-time domain, which was not described in previous studies. Using a modified PBHTM, Lakhssassi *et al.* (Lakhssassi et al., 2010) analyzed the effects of the thermal diffusivity and the temperature-dependent perfusion component on the thermal behavior of the biological system using both analytical and numerical approaches.

Although PBHTM has been applied mostly amongst other bio-heat models due to its simplicity and applicability, it is not easy to obtain analytical solutions for complex tissues. To address this, various numerical methods, such as finite element, finite difference, LBM and Monte Carlo methods have been applied to solve PBHTM equations. In particular, the

use of the LBM has increased widely because of its simple calculation procedure and and easiness of implementation and handling complex geometries as compared to conventional numerical methods. Lahonian and Golneshan (Lahonian and Golneshan, 2011) applied a three-dimensional LBM to solve the equation for PBHTM and predicted the temperature distribution in a spherical tissue during magnetic fluid hyperthermia by considering the effect of blood perfusion, metabolism and MNP heat sources in the modeling. This study showed that the LBM could solve the bio-heat transfer problems with an acceptable accuracy. Although PBHTM is easy to implement as compared to other bio-heat models, it is still less accurate and complicated for robust analytical models.

3.2. Thermal Wave Bio-heat transfer Model (TWBHTM)

The equation for the PBHTM is based on the classical Fourier's law which assumes that the velocity of thermal wave propagation in the homogeneous is infinite. However, this assumption may not be valid for the materials with a specific internal structure such as biological tissues, which have lengthy thermal relaxation time associated with a non-Fourier thermal behavior. For example, in the skin layer, the thermal relaxation time of skin caused by heat conduction can influence the temperature in the skin depth. In order to overcome the shortcoming of PBHTM, Liu et al. (Liu J et al., 1995) proposed TWBHTM by incorporating a single-phase lagging parameter in the model based on the wave model of heat conduction equation by Cattaneo (Cattaneo, 1958) and Vernotte (Vernotte, 1958). This model can account for the delay effect of the local and temporary heat influx with respect to the temperature gradient.

The constitutive relationship for the thermal wave model is given as;

$$q\left(r, t+\tau_q\right) = -k\nabla T(r,t) \tag{21}$$

where τ_q is the relaxation time (or a phase-lag parameter) and represents time-shift between the heat flux and the temperature gradient.

Several research groups have applied TWBHTM to predict the thermal behavior of biological tissue induced by hyperthermia treatment. Liu *et al.* (Liu and Lin, 2010) used the hybrid numerical scheme based on the Laplace transform in connection with hyperbolic shape functions. This study could predict changes in temperature occurring in a two-layer concentric spherical tissue with the Gaussian distribution of heat source, along with the influences of relaxation time, blood perfusion rate, and heating strength on the thermal response in the tissue. Ahmadikia *et al.* (Ahmadikia et al., 2012) predicted the temperature distribution of skin tissue analytically by applying TWBHTM based on the Laplace transform to the single layer model of skin tissue. They demonstrated that TWBHTM could provide an improved prediction of thermal behavior during the laser-irradiated heating and at the initial phase of cooling process, compared to the prediction by PBTHM.

3.3. Dual Phase Lag Bio-heat transfer Model (DPLBHTM)

Although TWBHTM is more accurate and generalized than PBTHM, it still has a limitation in describing heat transfer processes occurring at micro and nano scales. In view of this, DPLBHTM was proposed to further refine the non-Fourier thermal behavior of biological

tissues associated with their non-homogeneous inner structures (Tzou, 1997). This model enables a more accurate prediction of temperature distribution in living tissue by incorporating the relaxation behavior of both the heat flux and temperature gradient during the heat transfer process. The dual-phase lag (DPL) constitutive equation for DPLBHTM can be derived by considering a phase lag for temperature gradient in the constitutive equation of TWBHTM (Kumar et al., 2015);

$$q(r, t + \tau_q) = -k \nabla T(r, t + \tau_T) \tag{22}$$

where the temperature gradient at location r at time $t + \tau_t$ is related to the heat flux at time $t + \tau_q$.

Zhou *et al.* (Zhou et al., 2009) applied a two-dimensional axisymmetric DPL model to describe heat transfer in living biological tissues with nonhomogeneous inner structures. This model predicted variations of the non-uniform distributions of temperature and demonstrated that the multi-dimensional effects of thermal wave and diffusion cannot be negligible for a local heating with the heated spot smaller than the tissue bulk. Liu and Chen (Liu and Chen, 2009) have applied the DPLBHTM for thermal analysis of the dual-layer concentric spherical system, mimicking a small tumor surrounded by the healthy tissue, during the treatment of MNP hyperthermia. They examined the influences of various parameters, such as lag times, metabolic heat, blood perfusion rates and other physiological parameters, on the non-Fourier thermal response in tumor and normal tissues. However, DPLBHTM is still associated with mathematical difficulties in describing boundary conditions due to the difference in physiological and thermal properties for tissue with layered structures. To address this, a hybrid numerical method based on the Laplace transform and the modified discretization technique was introduced (Kuo-Chi et al., 2011; Liu and Cheng, 2008). Kumar *et al.* (Kumar et al., 2016) applied DPLBHTM for the layered tissue with Fourier and non-Fourier boundary conditions using the finite difference Legendre wavelet Galerkin approach. Their model could predict temperature profiles in a tumor tissue by choosing the appropriate parameters of the modified Gaussian heat source.

4. Applications, challenges, and future directions for the numerical modeling of MNP hyperthermia

4.1 Biomedical applications of bio-heat models for MNP hyperthermia

This section introduces the biomedical applications of bio-heat models, including PBHTM, TWBHTM, and DPLBHTM, for predicting thermal behaviors of living tissues, particularly for tumor tissue models, in response to MNP hyperthermia. Table 3 summarizes different bioheat models and solving techniques used for models of tumor diseases, including brain tumors, liver tumors, and breast tumors.

Brain tumor—A brain tumor is an intracranial solid that is caused by the growth of abnormal cells in the brain or spinal canal and responsible for substantial morbidity and mortality worldwide (Patel et al., 2019). Numerous studies including clinical trials have demonstrated the feasibility and efficacy of MNP hyperthermia as a therapeutic modality for

glioblastoma, a devastating form of brain tumor (Mahmoudi et al., 2018) (Fig. 5). However, it still necessitates the application of numerical models that can reliably predict temperature distribution as well as the potential risk of non-specific heating of healthy tissues, to ensure the safe application of MNP hyperthermia to the brain tissue.

Rast and Harrison (Rast and Harrison, 2010) applied PBHTM for the computational modeling of electromagnetic and thermal effects of MNP hyperthermia using a multilayer model of the human head made up of perfused dermal and skeletal layers and a grey-matter region surrounding a composite region of tumor tissue and MNPs. They used the solution of Maxwell's equation in a model of tumor and surrounding healthy tissue as an input to the equation of PBMTM and solved the equation using the finite difference time domain method. This study revealed that the temperature rise in the tumor region was dependent on the rate of blood perfusion. Bellizi *et al.* (Bellizzi et al., 2016) applied PBHTM for the numerical modeling of MNP hyperthermia for a human brain tumor. Their numerical model predicted that the MNP dosage could be maintained at a minimum by increasing the product of field strength and applied frequency by two to four times.

Liver tumor—Liver cancer is the third leading cause of cancer-related deaths worldwide, in which hepatocellular carcinoma (HCC) represents approximately 90% of all cases (Balogh et al., 2016). Attar *et al.* (Attar et al., 2014) numerically analyzed temperature profiles in porcine liver tissue to MNP hyperthermia by assuming the heterogeneous dispersion of MNPs, which was in good agreement with experimental data. In their subsequent study (Attar et al., 2016), they investigated whether the thermo-viscoelastic behavior of tissue could provide an improved prediction of temperature profiles in tumorous liver tissue. They validated their results from numerical analysis by comparing them with experimental results, which revealed that blood perfusion, exposure time and MNP dosage are the three important factors influencing temperature profiles. Additionally, this study further revealed that the bio-heat model based on the viscoelastic property of liver tissue could provide a better prediction of temperature distribution than the one based on the elastic property of tissue. Suleman and Riaz (Suleman and Riaz, 2020) presented a finite element model for the thermal analysis of liver tumor tissue, in which they could predict the pressure, velocity, concentration, temperature distribution, and the fraction of damaged tumor during the treatment using COMSOL Multiphysics (Fig. 6).

Breast tumor—Breast cancer is the most common type of cancer among women and is a metastatic type of cancer, which can commonly transfer to distant organs such as the liver, lung and brain (Sun et al., 2017). Miaskowski and Sawicki (Miaskowski and Sawicki, 2013) have presented a numerical model to estimate the temperature distribution in the breast tissue that mimics breast cancer during MNP hyperthermia by employing a PBHTM. Miaskowski and Subramanian (Miaskowski and Subramanian, 2019) presented a more advanced numerical model by using an anatomically correct breast tissue derived from magnetic resonance imaging (MRI). They predicted the temperature distribution within the realistic breast phantom by applying PBHTM with Robin's boundary conditions. This study revealed that the hot spots could happen with higher temperature gradients due to the eddy

current effects associated with the anatomical structure of breast tissues, suggesting the importance of applying anatomically correct tissue models in the numerical modeling.

The prediction of cell death—For the clinical translation of MNP hyperthermia for cancer treatment, it is important to predict the extent of cell death for the given conditions of MNP hyperthermia. Pearce *et al.* (Pearce et al., 2017) presented a numerical model coupled with experimental findings to predict the heating effectiveness of MNP hyperthermia against cancer cells. The inclusion of multiple biological processes involving cell death in the numerical model enabled the prediction on the treatment efficacy. Subramanian *et al.* (Subramanian et al., 2016) carried out numerical simulation by using the SEMCADE X software to predict the thermal dose for the death of cancer cells.

4.2 Challenges and perspectives for future study

Recent pre-clinical and clinical studies of MNP hyperthermia have demonstrated that this therapy could be an effective therapeutic modality, especially for cancer treatment in combination with conventional chemo or radiation therapy (Breugom et al., 2015; Iliadis and Barbolosi, 2000; Neukam and Stelzle, 2010; Sridhar and Symonds, 2009). This technology is also emerging as a new therapeutic platform for treating tissue infections (Kim et al., 2013). However, despite the promise of MNP hyperthermia as a therapeutic platform, a safety risk arising from potential thermal damage effects on the healthy tissue has been the primary concern of translating this therapy to clinics. From a clinical point of view, this necessitates the development and application of reliable bio-heat models for predicting the thermal effects of MNP hyperthermia on living tissues, which can enhance our ability to predict a potential safety risk of this therapy.

Although recently developed bio-heat models for MNP hyperthermia have greatly improved our understanding of heat transfer phenomena in living tissue, the use of more reliable thermal models is still warranted. First, it is necessary to obtain a more precise understanding on the spatial distribution of MNPs in the tissue, as an input parameter of a bio-heat model. As discussed above, the concentration and spatial distribution of MNPs as well as the properties of tissue in which the MNPs are dispersed are critical factors that can significantly influence heat transfer phenomena within the target tissue. However, it is still challenging to determine the spatial distribution of MNPs at micro and nano scales once they are injected into the tissue. The MNP hyperthermia combined with an advanced imaging tool such as magnetic particle imaging (MPI) may enable the reliable prediction of MNP dispersion in the tissue (Tay et al., 2018). The MPI was shown to exhibit better spatial resolution and sensitivity than conventional imaging modalities including MRI (Wu et al., 2019). Additionally, the development of numerical models for predicting the transport and diffusion of MNPs during and after the injections of MNPs to the target region is necessary. Second, although recently developed bio-heat models enable the prediction of heat transfer phenomena associated with thermal conduction and convection between vascular system and surrounding tissue (Lahonian and Golneshan, 2011; Majee and Shit, 2017; Tang et al., 2018), many studies for the thermal analysis of MNP hyperthermia have been based on tissue models with a simplified tissue geometry and thermal property. Since the heat transfer phenomena in living tissue is influenced by the geometric factors of tissues, such as non-

homogeneity (Zhou et al., 2009), multi-layered property (Kumar et al., 2016), and irregular shapes (Lahonian and Golneshan, 2011), it may be necessary to obtain more accurate information on the geometry and thermal property of target tissue for the modeling. Third, more accurate information about blood perfusion is important as a critical parameter for bio-heat equations of thermal models due to its major role in conferring cooling effects. Thus, a realistic thermal model should properly incorporate cooling effects arising from the vasculature networks within a target tissue. For example, a tissue model based on detailed analysis of the vascular architecture such as three-dimensional discrete vasculature (DIVA) networks may enable more reliable predictions of heat transfer between blood vessels and tissues (Hristov, 2019; Kotte et al., 1996).

5. Conclusions

In order to achieve desired thermal toxicity against target cells, while avoiding thermal damage to the surrounding healthy tissue, it is critical to reliably predict temperature distribution in the affected living tissue through numerical modeling. Indeed, numerous studies on the analytical and numerical modeling for MNP hyperthermia have significantly contributed to our understanding on the safe application of the therapy as well as improving its therapeutic efficacy. Due to the importance of precisely predicting SLP as an input parameter for the equation of bio-heat models of MNP hyperthermia, various analytical and empirical methods for determining SLP have been proposed. The estimation of SLP can be improved by properly considering various parameters, such as the type, concentration, and distribution of MNPs, characteristics of carrier fluid, and the strength and frequency of AMF. In order to better predict the thermal behaviors of living tissue in response to MNP hyperthermia, refined bio-heat models, that incorporate the effects of blood perfusion and metabolic heat generation, such as PBHTM, TWBHTM and DPLBHTM have been applied for biomedical applications, particularly for models of tumor diseases. Future studies should be directed towards further refining the bio-heat models based on the accurate information on the spatial distribution of MNPs as well as tissue properties and anatomy including vasculature networks. This will enable the reliable prediction of the spatiotemporal distribution of temperature in the target tissue in response to MNP hyperthermia, which will ensure the safe application of this therapy.

Acknowledgment

This research was supported by the Basic Science Research Program, through the National Research Foundation of Korea (NRF-2017R1D1A1B03028368), funded by the Ministry of Education (to HK). This research was also supported in part by the National Institute of Health (R01NR015674) (to MK).

References

Abenojar EC, Wickramasinghe S, Bas-Concepcion J, Samia ACS, 2016 Structural effects on the magnetic hyperthermia properties of iron oxide nanoparticles. Prog. Nat. Sci. 26, 440–448. 10.1016/j.pnsc.2016.09.004

Ahmadikia H, Moradi A, Fazlali R, Parsa AB, 2012 Analytical solution of non-Fourier and Fourier bioheat transfer analysis during laser irradiation of skin tissue. J. Mech. Sci. Technol. 26, 1937–1947. 10.1007/s12206-012-0404-9

Alumutairi L, Yu B, Filka M, Nayfach J, Kim M-H, 2020 Mild magnetic nanoparticle hyperthermia enhances the susceptibility of Staphylococcus aureus biofilm to antibiotics. Int. J. Hyperth. 37, 66–75. 10.1080/02656736.2019.1707886

Andreu I, Natividad E, 2013 Accuracy of available methods for quantifying the heat power generation of nanoparticles for magnetic hyperthermia. Int. J. Hyperthermia 29, 739–751. 10.3109/02656736.2013.826825 [PubMed: 24001056]

Arkin H, Xu LX, Holmes KR, 1994 Recent developments in modeling heat transfer in blood perfused tissues. IEEE Trans. Biomed. Eng. 41, 97–107. 10.1109/10.284920 [PubMed: 8026856]

Arora D, Skliar M, Roemer RB, 2002 Model-predictive control of hyperthermia treatments. IEEE Transactions on Biomedical Engineering 49, 629–639. [PubMed: 12083297]

Astefanoaei I, Stancu A, 2017 Modeling of the Temperature Field in the Magnetic Hyperthermia, in: Numerical Simulations in Engineering and Science. IntechOpen.

Attar MM, Haghpanahi M, Amanpour S, Mohaqeq M, 2014 Analysis of bioheat transfer equation for hyperthermia cancer treatment. J. Mech. Sci. Technol. 28, 763–771. 10.1007/s12206-013-1141-4

Attar MM, Haghpanahi M, Shahverdi H, Imam A, 2016 Thermo-mechanical analysis of soft tissue in local hyperthermia treatment. J. Mech. Sci. Technol. 30, 1459–1469. 10.1007/s12206-015-1053-6

Bakoglidis KD, Simeonidis K, Sakellari D, Stefanou G, Angelakeris M, 2012 Size-Dependent Mechanisms in AC Magnetic Hyperthermia Response of Iron-Oxide Nanoparticles. IEEE Trans. Magn. 48, 1320–1323. 10.1109/TMAG.2011.2173474

Balogh J, Victor D, Asham EH, Burroughs SG, Boktour M, Saharia A, Li X, Ghobrial M, Monsour H, 2016 Hepatocellular carcinoma: a review. J Hepatocell Carcinoma Volume 3, 41–53. 10.2147/JHC.S61146 [PubMed: 27785449]

Bekovic M, Hamler A, 2010 Determination of the Heating Effect of Magnetic Fluid in Alternating Magnetic Field. IEEE T .Magn. 46, 552–555. 10.1109/TMAG.2009.2033944

Beković M, Trbušić M, Gyergyek S, Trlep M, Jesenik M, Szabo P, Hamler A, 2019 Numerical Model for Determining the Magnetic Loss of Magnetic Fluids. Materials 12, 591 10.3390/ma12040591

Bellizzi G, Bucci OM, Chirico G, 2016 Numerical assessment of a criterion for the optimal choice of the operative conditions in magnetic nanoparticle hyperthermia on a realistic model of the human head. Int. J. Hyperthermia 32, 688–703. 10.3109/02656736.2016.1167258 [PubMed: 27268850]

Bordelon DE, Cornejo C, Grüttner C, Westphal F, DeWeese TL, Ivkov R, 2011 Magnetic nanoparticle heating efficiency reveals magneto-structural differences when characterized with wide ranging and high amplitude alternating magnetic fields. J. Appl. Phys. 109, 124904 10.1063/1.3597820

Breugom AJ, Swets M, Bosset J-F, Collette L, Sainato A, Cionini L, Glynne-Jones R, Counsell N, Bastiaannet E, van den Broek CBM, Liefers G-J, Putter H, van de Velde CJH, 2015 Adjuvant chemotherapy after preoperative (chemo)radiotherapy and surgery for patients with rectal cancer: a systematic review and meta-analysis of individual patient data. Lancet Oncol 16, 200–207. 10.1016/S1470-2045(14)71199-4 [PubMed: 25589192]

Brinck H, Werner J, 1995 Use of vascular and non-vascular models for the assessment of temperature distribution during induced hyperthermia. Int. J. Hyperth. 11, 615–626. 10.3109/02656739509022494

Brinck H, Werner J, 1994 Estimation of the Thermal Effect of Blood Flow in a Branching Countercurrent Network Using a Three-Dimensional Vascular Model. J. Biomech. Eng. 116, 324–330. 10.1115/1.2895738 [PubMed: 7799635]

Carrey J, Mehdaoui B, Respaud M, 2011 Simple models for dynamic hysteresis loop calculations of magnetic single-domain nanoparticles: Application to magnetic hyperthermia optimization. J. Appl. Phys. 109, 083921 10.1063/1.3551582

Cattaneo C, 1958 A form of heat-conduction equations which eliminates the paradox of instantaneous propagation. Comptes Rendus 247, 431.

Cervadoro A, Giverso C, Pande R, Sarangi S, Preziosi L, Wosik J, Brazdeikis A, Decuzzi P, 2013 Design Maps for the Hyperthermic Treatment of Tumors with Superparamagnetic Nanoparticles. PLoS ONE 8, e57332 10.1371/journal.pone.0057332 [PubMed: 23451208]

Chang D, Lim M, Goos JACM, Qiao R, Ng YY, Mansfeld FM, Jackson M, Davis TP, Kavallaris M, 2018 Biologically Targeted Magnetic Hyperthermia: Potential and Limitations. Front. Pharmacol. 9 10.3389/fphar.2018.00831

Cobianchi M, Guerrini A, Avolio M, Innocenti C, Corti M, Arosio P, Orsini F, Sangregorio C, Lascialfari A, 2017 Experimental determination of the frequency and field dependence of Specific Loss Power in Magnetic Fluid Hyperthermia. J. Magn. Magn. Mater. 444, 154–160. 10.1016/j.jmmm.2017.08.014

Deatsch AE, Evans BA, 2014 Heating efficiency in magnetic nanoparticle hyperthermia. Journal of Magnetism and Magnetic Materials 354, 163–172. 10.1016/j.jmmm.2013.11.006

Dennis CL, Ivkov R, 2013 Physics of heat generation using magnetic nanoparticles for hyperthermia. Int. J. Hyperth. 29, 715–729. 10.3109/02656736.2013.836758

Di Corato R, Espinosa A, Lartigue L, Tharaud M, Chat S, Pellegrino T, Ménager C, Gazeau F, Wilhelm C, 2014 Magnetic hyperthermia efficiency in the cellular environment for different nanoparticle designs. Biomaterials 35, 6400–6411. 10.1016/j.biomaterials.2014.04.036 [PubMed: 24816363]

Dutz S, Hergt R, 2014 Magnetic particle hyperthermia—a promising tumour therapy? Nanotechnology 25, 452001. [PubMed: 25337919]

Engelmann UM, Shasha C, Teeman E, Slabu I, Krishnan KM, 2019 Predicting size-dependent heating efficiency of magnetic nanoparticles from experiment and stochastic Néel-Brown Langevin simulation. J. Magn. Magn. Mater. 471, 450–456. 10.1016/j.jmmm.2018.09.041

Gilchrist RK, Medal R, Shorey WD, Hanselman RC, Parrott JC, Taylor CB, 1957 Selective inductive heating of lymph nodes. Ann. Surg. 146, 596. [PubMed: 13470751]

Giustini AJ, Ivkov R, Hoopes PJ, 2009 An in vivo transmission electron microscopy study of injected dextran-coated iron-oxide nanoparticle location in murine breast adenocarcinoma tumors versus time, in: Ryan TP (Ed.), Presented at the SPIE BiOS: Biomed. Opt, San Jose, CA, p. 71810M 10.1117/12.809868

Golneshan AA, Lahonian M, 2011 The effect of magnetic nanoparticle dispersion on temperature distribution in a spherical tissue in magnetic fluid hyperthermia using the lattice Boltzmann method. Int. J. Hyperthermia 27, 266–274. 10.3109/02656736.2010.519370 [PubMed: 21501028]

Guardia P, Di Corato R, Lartigue L, Wilhelm C, Espinosa A, Garcia-Hernandez M, Gazeau F, Manna L, Pellegrino T, 2012 Water-Soluble Iron Oxide Nanocubes with High Values of Specific Absorption Rate for Cancer Cell Hyperthermia Treatment. ACS Nano 6, 3080–3091. 10.1021/nn2048137 [PubMed: 22494015]

Habash RW, Bansal R, Krewski D, Alhafid HT, 2006 Thermal therapy, part 1: an introduction to thermal therapy. Critical Reviews™ in Biomedical Engineering 34.

Habib AH, Ondeck CL, Chaudhary P, Bockstaller MR, McHenry ME, 2008 Evaluation of iron-cobalt/ferrite core-shell nanoparticles for cancer thermotherapy. J. Appl. Phys. 103, 07A307 10.1063/1.2830975

Hergt R, Andra W, d'Ambly CG, Hilger I, Kaiser WA, Richter U, Schmidt H-G, 1998 Physical limits of hyperthermia using magnetite fine particles. IEEE T .Magn. 34, 3745–3754. 10.1109/20.718537

Hristov J, 2019 Bio-Heat Models Revisited: Concepts, Derivations, Nondimensalization and Fractionalization Approaches. Front. Phys. 7 10.3389/fphy.2019.00189

Huang H-W, Liauh C-T, Shih T-C, Horng T-L, Lin W-L, 2010 Significance of blood vessels in optimization of absorbed power and temperature distributions during hyperthermia. Int. J. Heat Mass Transf. 53, 5651–5662. 10.1016/j.ijheatmasstransfer.2010.08.017

Iliadis A, Barbolosi D, 2000 Optimizing Drug Regimens in Cancer Chemotherapy by an Efficacy–Toxicity Mathematical Model. Comput. Biomed. Res. 33, 211–226. 10.1006/cbmr.2000.1540 [PubMed: 10860586]

Johannsen M, Gneveckow U, Taymoorian K, Thiesen B, Waldöfner N, Scholz R, Jung K, Jordan A, Wust P, Loening SA, 2007 Morbidity and quality of life during thermotherapy using magnetic nanoparticles in locally recurrent prostate cancer: Results of a prospective phase I trial. Int. J. Hyperth. 23, 315–323. 10.1080/02656730601175479

Johannsen M, Thiesen B, Wust P, Jordan A, 2010 Magnetic nanoparticle hyperthermia for prostate cancer. International Journal of Hyperthermia 26, 790–795. 10.3109/02656731003745740 [PubMed: 20653418]

Kalambur VS, Han B, Hammer BE, Shield TW, Bischof JC, 2005 In vitro characterization of movement, heating and visualization of magnetic nanoparticles for biomedical applications. Nanotechnology 16, 1221.

Kappiyoor R, Liangruksa M, Ganguly R, Puri IK, 2010 The effects of magnetic nanoparticle properties on magnetic fluid hyperthermia. J. Appl. Phys. 108, 094702 10.1063/1.3500337

Kasyutich O, Desautels RD, Southern BW, van Lierop J, 2010 Novel Aspects of Magnetic Interactions in a Macroscopic 3D Nanoparticle-Based Crystal. Phys. Rev. Lett 104 10.1103/PhysRevLett.104.127205

Kim M-H, Yamayoshi I, Mathew S, Lin H, Nayfach J, Simon SI, 2013 Magnetic Nanoparticle Targeted Hyperthermia of Cutaneous Staphylococcus aureus Infection. Ann Biomed Eng 41, 598–609. 10.1007/s10439-012-0698-x [PubMed: 23149904]

Kotte A, Leeuwen G, van Bree, de J, Koijk, van der J, Crezee H, Lagendijk J, 1996 A description of discrete vessel segments in thermal modelling of tissues. Phys. Med. Biol. 41, 865–884. 10.1088/0031-9155/41/5/004 [PubMed: 8735254]

Kumar D, Kumar P, Rai KN, 2016 A study on DPL model of heat transfer in bi-layer tissues during MFH treatment. Comput. Biol. Med. 75, 160–172. 10.1016/j.compbiomed.2016.06.002 [PubMed: 27289539]

Kumar P, Kumar D, Rai KN, 2015 A numerical study on dual-phase-lag model of bio-heat transfer during hyperthermia treatment. J. Therm. Biol. 49–50, 98–105. 10.1016/j.jtherbio.2015.02.008

Kuo-Chi L, Po-Jen C, Yan-Nan W, 2011 Analysis of non-Fourier thermal behavior for multi-layer skin model. Therm. Sci. 15, 61–67. 10.2298/TSCI11S1061L

Lagendijk JJW, 1982 The influence of bloodflow in large vessels on the temperature distribution in hyperthermia. Phys. Med. Biol. 27, 17–23. 10.1088/0031-9155/27/1/002 [PubMed: 7071137]

Lagendijk JJW, Hofman P, Schipper J, 1988 Perfusion analyses in advanced breast carcinoma during hyperthermia. Int. J. Hyperth. 4, 479–495. 10.3109/02656738809027693

Lahonian M, Golneshan AA, 2011 Numerical Study of Temperature Distribution in a Spherical Tissue in Magnetic Fluid Hyperthermia Using Lattice Boltzmann Method. IEEE Trans. Nanobiosci. 10, 262–268. 10.1109/TNB.2011.2177100

Lakhssassi A, Kengne E, Semmaoui H, 2010 Modifed pennes' equation modelling bio-heat transfer in living tissues: analytical and numerical analysis. Natural Science 02, 1375–1385. 10.4236/ns.2010.212168

Lanier OL, Korotych OI, Monsalve AG, Wable D, Savliwala S, Grooms NWF, Nacea C, Tuitt OR, Dobson J, 2019 Evaluation of magnetic nanoparticles for magnetic fluid hyperthermia. Int. J. Hyperth. 36, 686–700. 10.1080/02656736.2019.1628313

Lévy M, Wilhelm C, Siaugue J-M, Horner O, Bacri J-C, Gazeau F, 2008 Magnetically induced hyperthermia: size-dependent heating power of γ-Fe $_2$ O $_3$ nanoparticles. J. Phys.: Condens. Matter 20, 204133 10.1088/0953-8984/20/20/204133 [PubMed: 21694262]

Li Z, Kawashita M, Araki N, Mistumori M, Hiraoka M, 2011 Effect of particle size of magnetite nanoparticles on heat generating ability under alternating magnetic field. Bioceram. Dev. Appl. 1.

Lin C-T, Liu K-C, 2009 Estimation for the heating effect of magnetic nanoparticles in perfused tissues. International Communications in Heat and Mass Transfer 36, 241–244.

Liu J, Ren Z, Wang C, 1995 Interpretation of living tissue's temperature oscillations by thermal wave theory. Chinese Science Bulletin 21.

Liu K-C, Chen H-T, 2009 Analysis for the dual-phase-lag bio-heat transfer during magnetic hyperthermia treatment. Int. J. Heat Mass Transf. 52, 1185–1192. 10.1016/j.ijheatmasstransfer.2008.08.025

Liu K-C, Cheng P-J, 2008 Finite Propagation of Heat Transfer in a Multilayer Tissue. J. Thermophys. Heat Transf. 22, 775–782. 10.2514/1.37267

Liu K-C, Lin C-N, 2010 Temperature Prediction for Tumor Hyperthermia with the Behavior of Thermal Wave. Numer. Heat Tranf. A-Appl 58, 819–833. 10.1080/10407782.2010.523330

Liu X, Zhang Yifan, Wang Y, Zhu W, Li G, Ma X, Zhang Yihan, Chen S, Tiwari S, Shi K, Zhang S, Fan HM, Zhao YX, Liang X-J, 2020 Comprehensive understanding of magnetic hyperthermia for improving antitumor therapeutic efficacy. Theranostics 10, 3793–3815. 10.7150/thno.40805 [PubMed: 32206123]

Lyutyy TV, Denisov SI, Peletskyi, Yu A, Binns C, 2015 Energy dissipation in single-domain ferromagnetic nanoparticles: Dynamical approach. Phys. Rev. B 91 10.1103/PhysRevB.91.054425

Mahmoudi K, Bouras A, Bozec D, Ivkov R, Hadjipanayis C, 2018 Magnetic hyperthermia therapy for the treatment of glioblastoma: a review of the therapy's history, efficacy and application in humans. Int. J. Hyperth 34, 1316–1328. 10.1080/02656736.2018.1430867

Mahmoudi K, Hadjipanayis CG, 2014 The application of magnetic nanoparticles for the treatment of brain tumors. Front. Chem. 2 10.3389/fchem.2014.00109

Maier-Hauff K, Rothe R, Scholz R, Gneveckow U, Wust P, Thiesen B, Feussner A, von Deimling A, Waldoefner N, Felix R, Jordan A, 2007 Intracranial Thermotherapy using Magnetic Nanoparticles Combined with External Beam Radiotherapy: Results of a Feasibility Study on Patients with Glioblastoma Multiforme. J. Neuro-Oncol 81, 53–60. 10.1007/s11060-006-9195-0

Maier-Hauff K, Ulrich F, Nestler D, Niehoff H, Wust P, Thiesen B, Orawa H, Budach V, Jordan A, 2011 Efficacy and safety of intratumoral thermotherapy using magnetic iron-oxide nanoparticles combined with external beam radiotherapy on patients with recurrent glioblastoma multiforme. J. Neuro-Oncol. 103, 317–324. 10.1007/s11060-010-0389-0

Majee S, Shit GC, 2017 Numerical investigation of MHD flow of blood and heat transfer in a stenosed arterial segment. J. Magn. Magn. Mater. 424, 137–147. 10.1016/j.jmmm.2016.10.028

Matsumine A, Kusuzaki K, Matsubara T, Shintani K, Satonaka H, Wakabayashi T, Miyazaki S, Morita K, Takegami K, Uchida A, 2007 Novel hyperthermia for metastatic bone tumors with magnetic materials by generating an alternating electromagnetic field. Clin. Exp. Metastas. 24, 191–200. 10.1007/s10585-007-9068-8

Miaskowski A, Sawicki B, 2013 Magnetic Fluid Hyperthermia Modeling Based on Phantom Measurements and Realistic Breast Model. IEEE Trans. Biomed. Eng. 60, 1806–1813. 10.1109/TBME.2013.2242071 [PubMed: 23358949]

Miaskowski A, Subramanian M, 2019 Numerical Model for Magnetic Fluid Hyperthermia in a Realistic Breast Phantom: Calorimetric Calibration and Treatment Planning. Int. J. Mol. Sci. 20, 4644 10.3390/ijms20184644

Moreno R, Poyser S, Meilak D, Meo A, Jenkins S, Lazarov VK, Vallejo-Fernandez G, Majetich S, Evans RFL, 2020 The role of faceting and elongation on the magnetic anisotropy of magnetite Fe3O4 nanocrystals. Sci. Rep. 10 10.1038/s41598-020-58976-7

Natividad E, Castro M, Mediano A, 2008 Accurate measurement of the specific absorption rate using a suitable adiabatic magnetothermal setup. Appl. Phys. Lett. 92, 093116 10.1063/1.2891084

Neukam FW, Stelzle F, 2010 Laser tumor treatment in oral and maxillofacial surgery. Physics Procedia 5, 91–100. 10.1016/j.phpro.2010.08.125

Nieskoski MD, Trembly BS, 2014 Comparison of a Single Optimized Coil and a Helmholtz Pair for Magnetic Nanoparticle Hyperthermia. IEEE Trans. Biomed. Eng. 61, 1642–1650. 10.1109/TBME.2013.2296231 [PubMed: 24691525]

Patel AP, Fisher JL, Nichols E, Abd-Allah F, Abdela J, Abdelalim A, Abraha HN, Agius D, Alahdab F, Alam T, Allen CA, Anber NH, Awasthi A, Badali H, Belachew AB, Bijani A, Bjørge T, Carvalho F, Catalá-López F, Choi J-YJ, Daryani A, Degefa MG, Demoz GT, Do HP, Dubey M, Fernandes E, Filip I, Foreman KJ, Gebre AK, Geramo YCD, Hafezi-Nejad N, Hamidi S, Harvey JD, Hassen HY, Hay SI, Irvani SSN, Jakovljevic M, Jha RP, Kasaeian A, Khalil IA, Khan EA, Khang Y-H, Kim YJ, Mengistu G, Mohammad KA, Mokdad AH, Nagel G, Naghavi M, Naik G, Nguyen HLT, Nguyen LH, Nguyen TH, Nixon MR, Olagunju AT, Pereira DM, Pinilla-Monsalve GD, Poustchi H, Qorbani M, Radfar A, Reiner RC, Roshandel G, Safari H, Safiri S, Samy AM, Sarvi S, Shaikh MA, Sharif M, Sharma R, Sheikhbahaei S, Shirkoohi R, Singh JA, Smith M, Tabarés-Seisdedos R, Tran BX, Tran KB, Ullah I, Weiderpass E, Weldegwergs KG, Yimer EM, Zadnik V, Zaidi Z, Ellenbogen RG, Vos T, Feigin VL, Murray CJL, Fitzmaurice C, 2019 Global, regional, and national burden of brain and other CNS cancer, 1990–2016: a systematic analysis for the Global Burden of Disease Study 2016. Lancet Neurol. 18, 376–393. 10.1016/S1474-4422(18)30468-X [PubMed: 30797715]

Pearce JA, Petryk AA, Hoopes PJ, 2017 Numerical Model Study ofIn VivoMagnetic Nanoparticle Tumor Heating. IEEE Transactions on Biomedical Engineering 64, 2813–2823. [PubMed: 28362580]

Pennes HH, 1948 Analysis of tissue and arterial blood temperatures in the resting human forearm. J. Appl. Physiol. 1, 93–122. [PubMed: 18887578]

Purushotham S, Ramanujan RV, 2010 Modeling the performance of magnetic nanoparticles in multimodal cancer therapy. J. Appl. Phys. 107, 114701 10.1063/1.3432757

Rast L, Harrison JG, 2010 Computational Modeling of Electromagnetically Induced Heating of Magnetic Nanoparticle Materials for Hyperthermic Cancer Treatment. PIERS Online 6, 690–694. 10.2529/PIERS091218133748

Reis RF, Loureiro F, dos S, Lobosco M, 2016 3D numerical simulations on GPUs of hyperthermia with nanoparticles by a nonlinear bioheat model. J. Comput. Appl. Math. 295, 35–47. 10.1016/j.cam.2015.02.047

Rosensweig RE, 2002 Heating magnetic fluid with alternating magnetic field. J. Magn. Magn. Mater. 252, 370–374. 10.1016/S0304-8853(02)00706-0

Sanz B, Calatayud MP, Cassinelli N, Ibarra MR, Goya GF, 2015 Long-Term Stability and Reproducibility of Magnetic Colloids Are Key Issues for Steady Values of Specific Power Absorption over Time: Magnetic Colloids. Eur. J. Inorg. Chem 2015, 4524–4531. 10.1002/ejic.201500303

Sasayama T, Yoshida T, Tanabe K, Tsujimura N, Enpuku K, 2015 Hysteresis Loss of Fractionated Magnetic Nanoparticles for Hyperthermia Application. IEEE Transactions on Magnetics 51, 1–4. 10.1109/TMAG.2015.2438080 [PubMed: 26203196]

Shih T-C, Yuan P, Lin W-L, Kou H-S, 2007 Analytical analysis of the Pennes bioheat transfer equation with sinusoidal heat flux condition on skin surface. Med. Eng. Phys. 29, 946–953. 10.1016/j.medengphy.2006.10.008 [PubMed: 17137825]

Shubitidze F, Kekalo K, Stigliano R, Baker I, 2015 Magnetic nanoparticles with high specific absorption rate of electromagnetic energy at low field strength for hyperthermia therapy. J. Appl. Phys. 117, 094302 10.1063/1.4907915 [PubMed: 25825545]

Sridhar T, Symonds RP, 2009 Principles of chemotherapy and radiotherapy. Obstetrics, Gynaecology & Reproductive Medicine 19, 61–67.

Subramanian M, Pearce G, Guldu OK, Tekin V, Miaskowski A, Aras O, Unak P, 2016 A Pilot Study Into the Use of FDG-mNP as an Alternative Approach in Neuroblastoma Cell Hyperthermia. IEEE Transactions on NanoBioscience 15, 517–525. 10.1109/TNB.2016.2584543 [PubMed: 27824574]

Suleman M, Riaz S, 2020 In silico study of hyperthermia treatment of liver cancer using core-shell CoFe2O4@MnFe2O4 magnetic nanoparticles. J. Magn. Magn. Mater. 498, 166143 10.1016/j.jmmm.2019.166143

Sun Y-S, Zhao Z, Yang Z-N, Xu F, Lu H-J, Zhu Z-Y, Shi W, Jiang J, Yao P-P, Zhu H-P, 2017 Risk factors and preventions of breast cancer. Int. J. Biol. Sci. 13, 1387 10.7150/ijbs.21635

Tang Y, Flesch RCC, Jin T, 2017 Numerical analysis of temperature field improvement with nanoparticles designed to achieve critical power dissipation in magnetic hyperthermia. J. Appl. Phys. 122, 034702 10.1063/1.4994309

Tang Y, Flesch RCC, Zhang C, Jin T, 2018 Numerical analysis of the effect of non-uniformity of the magnetic field produced by a solenoid on temperature distribution during magnetic hyperthermia. J. Magn. Magn. Mater. 449, 455–460. 10.1016/j.jmmm.2017.10.076

Tay ZW, Chandrasekharan P, Chiu-Lam A, Hensley DW, Dhavalikar R, Zhou XY, Yu EY, Goodwill PW, Zheng B, Rinaldi C, Conolly SM, 2018 Magnetic Particle Imaging-Guided Heating in Vivo Using Gradient Fields for Arbitrary Localization of Magnetic Hyperthermia Therapy. ACS Nano 12, 3699–3713. 10.1021/acsnano.8b00893 [PubMed: 29570277]

Teran FJ, Casado C, Mikuszeit N, Salas G, Bollero A, Morales MP, Camarero J, Miranda R, 2012 Accurate determination of the specific absorption rate in superparamagnetic nanoparticles under non-adiabatic conditions. Appl. Phys. Lett. 101, 062413 10.1063/1.4742918

Thirion C, Wernsdorfer W, Demoncy N, Pascard H, Mailly D, 2002 Magnetization reversal by uniform rotation (Stoner–Wohlfarth model) in fcc cobalt nanoparticles, in: APS Meeting Abstracts.

Tzou DY, 1997 Macro-to microscale heat transfer: the lagging behavior. John Wiley & Sons.

Vernotte P, 1958 Les paradoxes de la theorie continue de l'equation de la chaleur. Compt. Rendu 246, 3154–3155.

Wadehra N, Gupta R, Prakash B, Sharma D, Chakraverty S, 2017 Biocompatible ferrite nanoparticles for hyperthermia: effect of polydispersity, anisotropy energy and inter-particle interaction. Mater. Res. Express 4, 025037 10.1088/2053-1591/aa5d93

Wang C, Hsu C-H, Li Z, Hwang L-P, Lin Y-C, Chou P-T, Lin Y-Y, 2017 Effective heating of magnetic nanoparticle aggregates for in vivo nano-theranostic hyperthermia. Int. J. Nanomed. Volume 12, 6273–6287. 10.2147/IJN.S141072

Wang Q, Deng ZS, Liu J, 2012 Theoretical evaluations of magnetic nanoparticle-enhanced heating on tumor embedded with large blood vessels during hyperthermia. J. Nanopart. Res. 14 10.1007/s11051-012-0974-6

Wang Q, Deng Z-S, Liu J, 2011 Effects of Nonuniform Tissue Properties on Temperature Prediction in Magnetic Nanohyperthermia. J.Nanotechnol.Eng.Med 2 10.1115/1.4003563

Wang S-Y, Huang S, Borca-Tasciuc D-A, 2013 Potential Sources of Errors in Measuring and Evaluating the Specific Loss Power of Magnetic Nanoparticles in an Alternating Magnetic Field. IEEE Trans. Magn. 49, 255–262. 10.1109/TMAG.2012.2224648

Wildeboer RR, Southern P, Pankhurst QA, 2014 On the reliable measurement of specific absorption rates and intrinsic loss parameters in magnetic hyperthermia materials. J. Phys. D-Appl. Phys. 47, 495003 10.1088/0022-3727/47/49/495003

Wu LC, Zhang Y, Steinberg G, Qu H, Huang S, Cheng M, Bliss T, Du F, Rao J, Song G, Pisani L, Doyle T, Conolly S, Krishnan K, Grant G, Wintermark M, 2019 A Review of Magnetic Particle Imaging and Perspectives on Neuroimaging. Am. J. Neuroradiol. 40, 206–212. 10.3174/ajnr.A5896 [PubMed: 30655254]

Wust Peter, Gneveckow U, Wust Peter, Gneveckow U, Johannsen M, Böhmer D, Henkel T, Kahmann F, Sehouli J, Felix R, Ricke J, Jordan A, 2006 Magnetic nanoparticles for interstitial thermotherapy – feasibility, tolerance and achieved temperatures. Int. J. Hyperth. 22, 673–685. 10.1080/02656730601106037

Zhou J, Zhang Y, Chen JK, 2009 An axisymmetric dual-phase-lag bioheat model for laser heating of living tissues. Int. J. Therm. Sci. 48, 1477–1485. 10.1016/j.ijthermalsci.2008.12.012

Highlights

- Mathematical models of MNP (Magnetic nanoparticles) hyperthermia are reviewed
- Various methods are discussed for evaluating the SLP (Specific Loss Power)
- Different factors that optimizing the SLP are reviewed for hyperthermia applications
- Bio-heat models and their applications are appraised for cancerous tumors
- Limitations and challenges for the modeling of hyperthermia are addressed

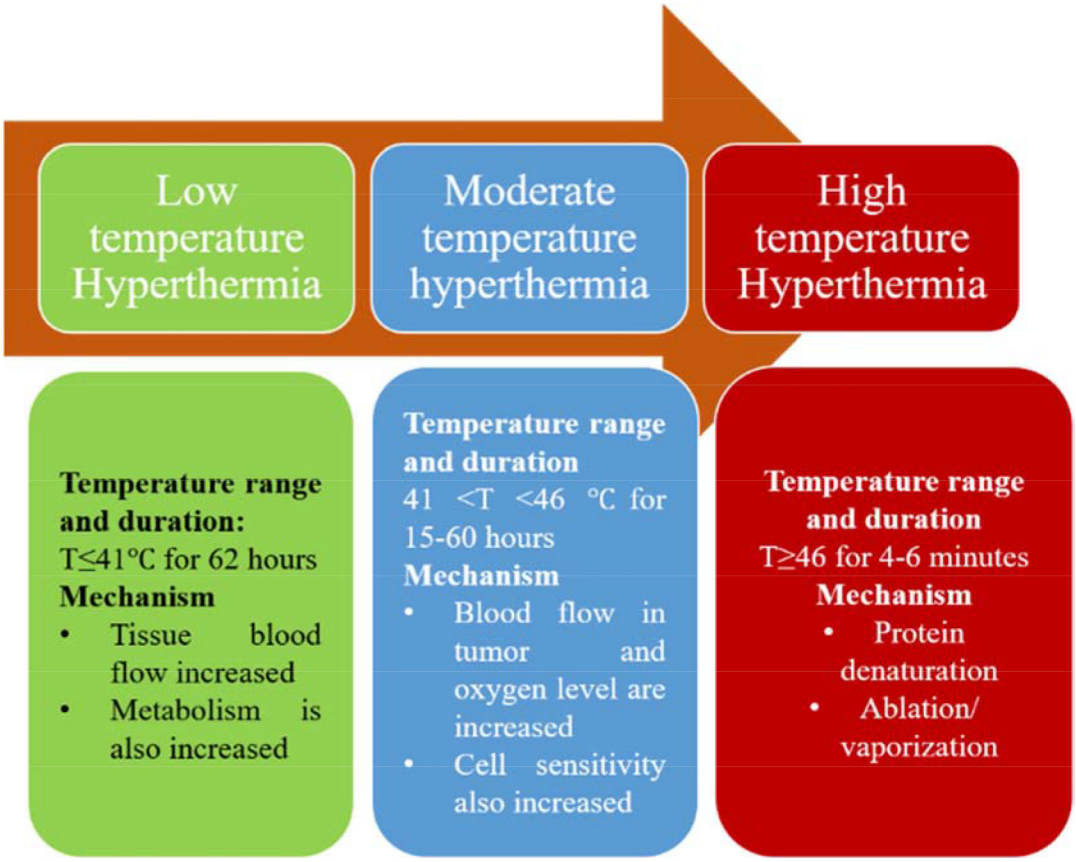

Fig. 1.
Categories of hyperthermia therapy based on the exposure time and temperature range.

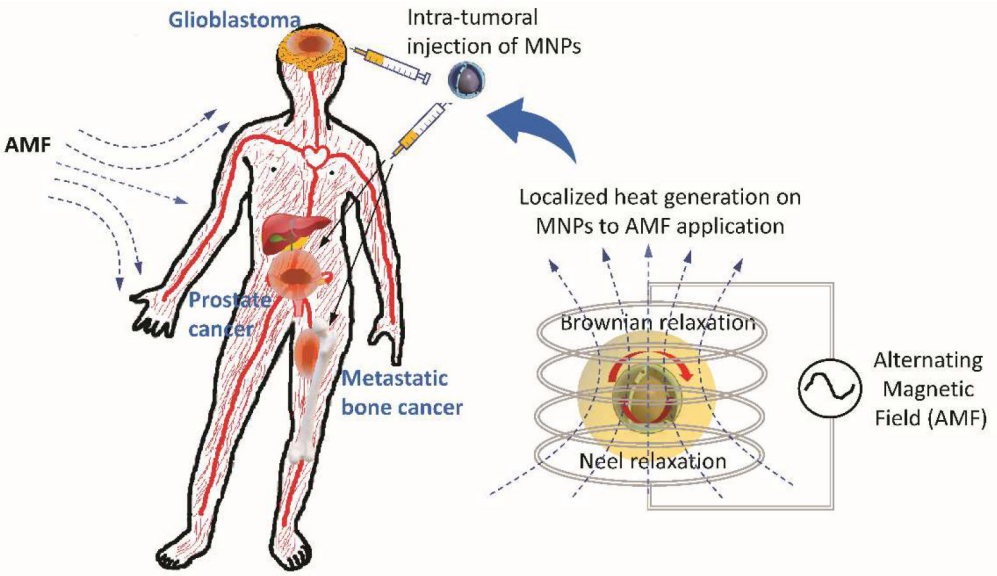

Fig. 2. Clinical applications of MNP hyperthermia for treating tumors.

Recent clinical trials for MNP hyperthermia demonstrated its safety and feasibility as an anti-cancer therapy for patients with glioblastoma, prostate cancer, and metastatic bone cancer. The principle of MNP hyperthermia is to achieve a localized increase in temperature in target cells or tissue by localized activation of MNPs upon exposure to a high frequency alternating magnetic field (AMF). The exposure of AMF to MNPs causes the conversion of electromagnetic energy into heat energy via mechanisms such as Brownian relaxation and Neel relaxation.

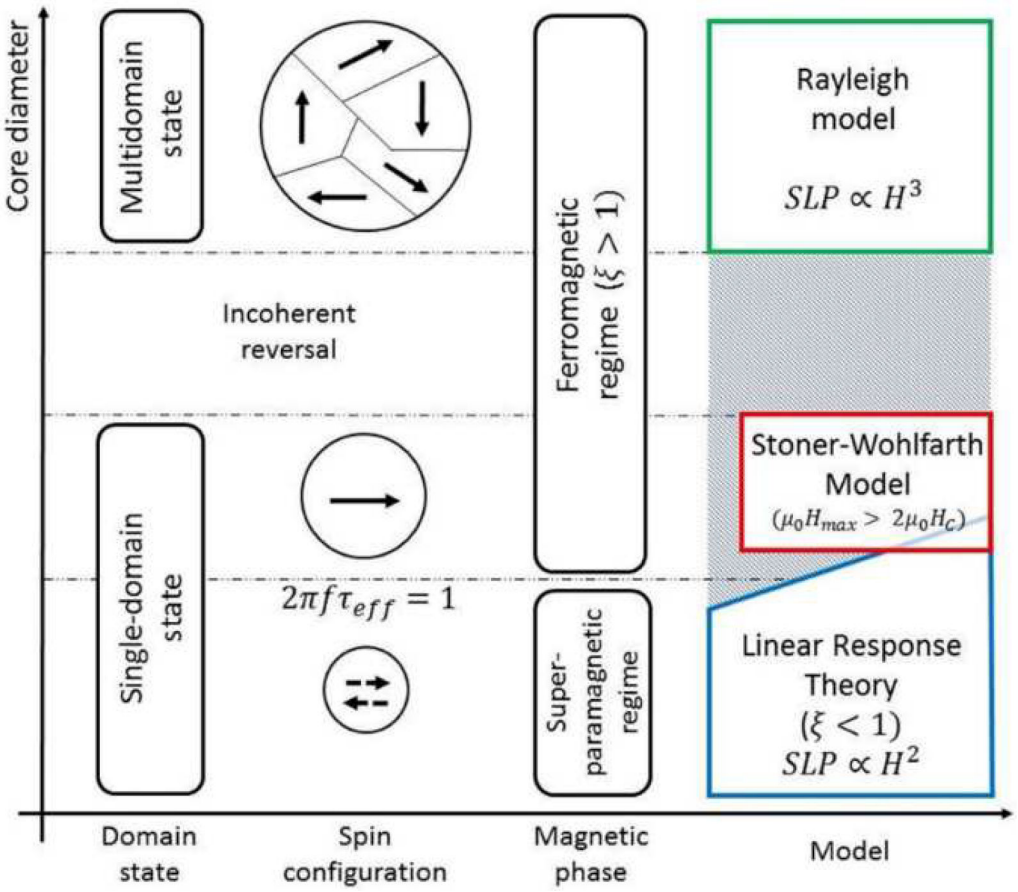

Fig. 3.
Graphical demonstration of the empirical models for calculation of SLP (Cobianchi et al., 2017).

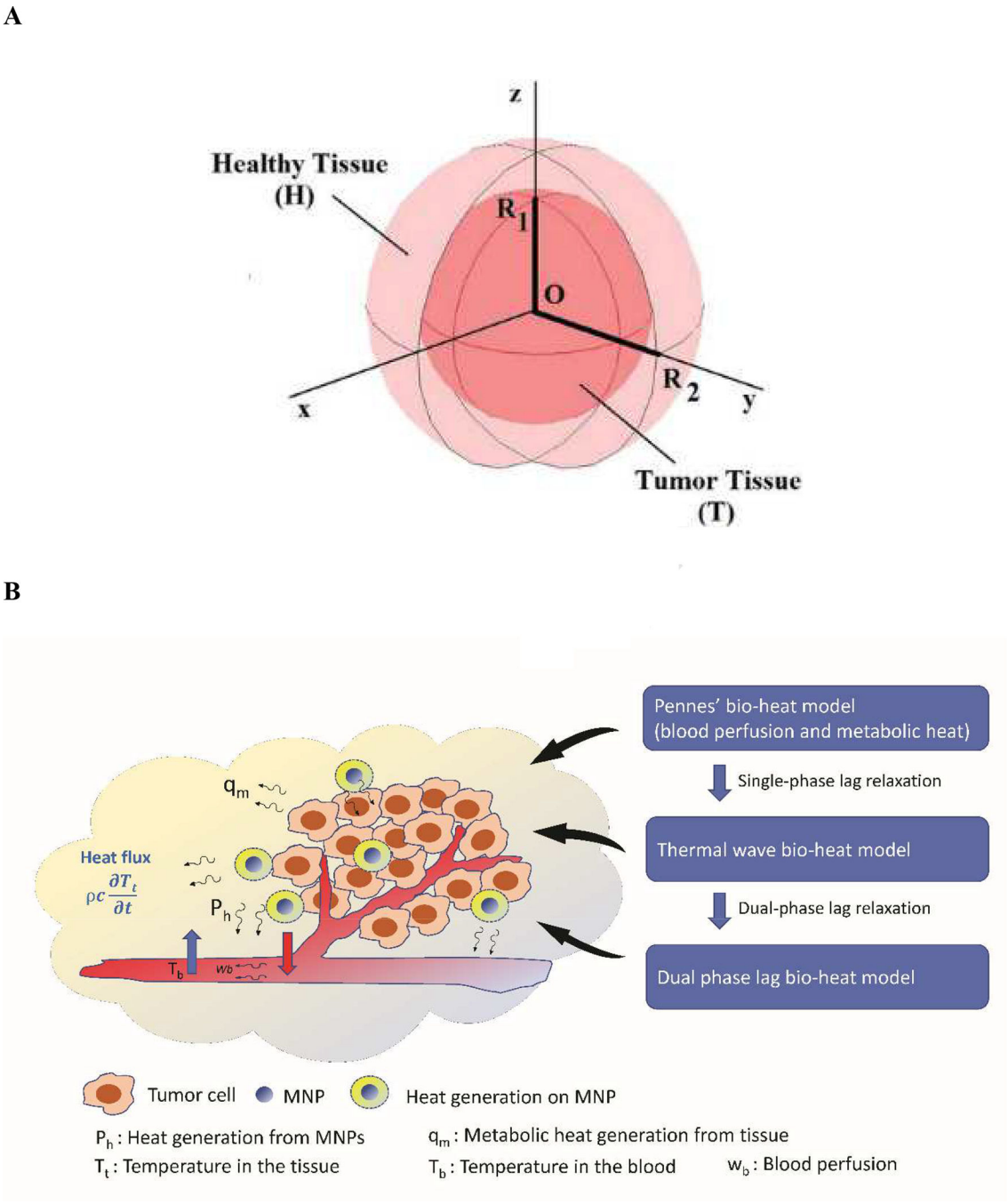

Fig. 4. A geometrical domain of tumor tissue for bio-heat models.

(A) A simplified domain of spherical tumor model, where a tumor is surrounded by a healthy tissue (Astefanoaei and Stancu, 2017). (B) A generalized geometrical domain of tumor tissue model for the application of bio-heat models (Penne's bio-heat model, Thermal wave bio-heat model, and Dual phase lag bio-heat model) by incorporating the effects of blood perfusion and metabolic heat generation, where cancerous tumor cells are surrounded by vasculature networks and healthy tissue.

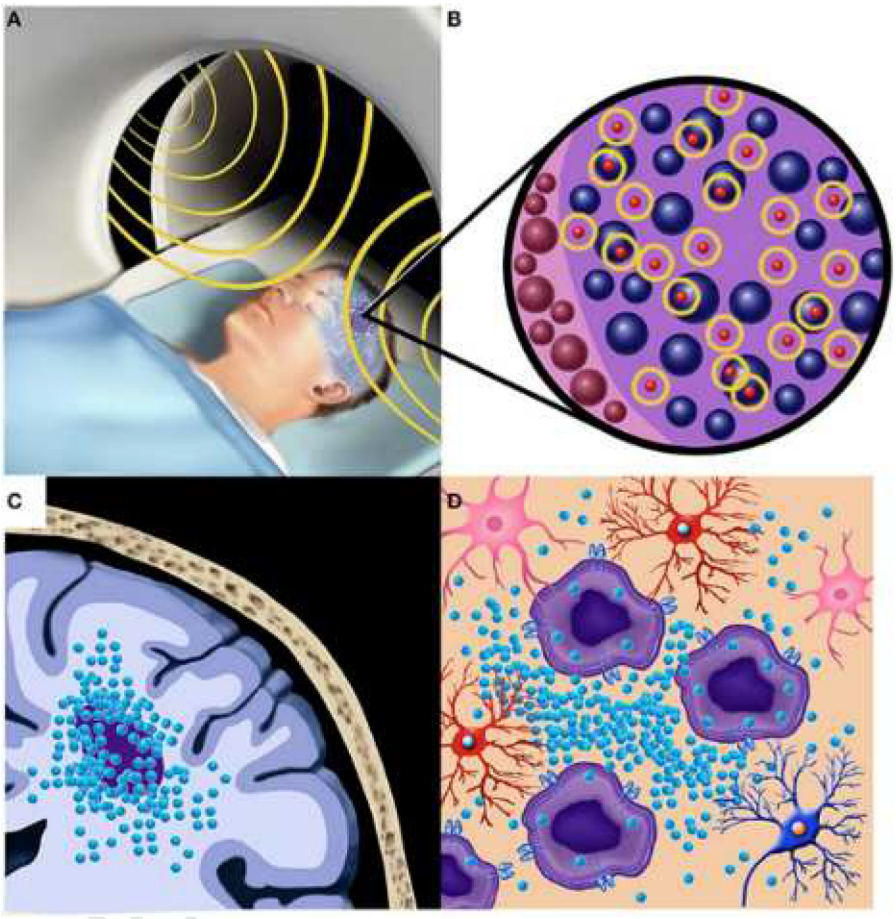

Fig. 5. A schematic of localized treatment of MNP hyperthermia for treating patient with malignant brain tumor.

(A) The patient undergoes an AMF (shown in yellow) for local hyperthermia following the intratumoral injection of MNPs. (B) Demonstration of MNPs (represented in red and encircled in yellow) adjacent with tumor cells providing the heating effect. (C) The localization of the MNPs within and adjacent to the brain tumor for providing a targeted therapeutic effect. (D) The preferential uptake of MNPs by tumor cells in a region of brain tumor surrounded by healthy normal cells (Mahmoudi and Hadjipanayis, 2014).

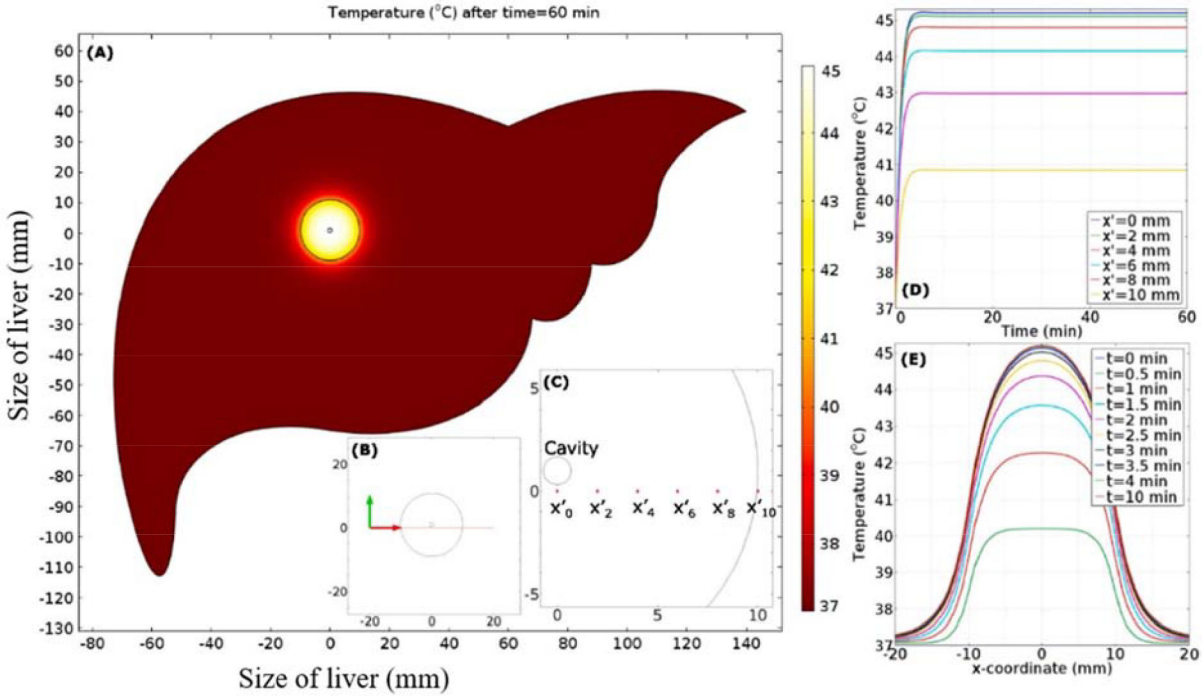

Fig. 6. Prediction of temperature distribution in a model of liver tissue during MNP hyperthermia by finite element analysis of bio-heat model.

(A) Temperature contours after 60 minutes of hyperthermia treatment. (B) Visual clue of line segment in liver tissue. (C) Visual clue of selected location in tumor region. (D) Temporal distribution of temperature as a function of location. (E) Spatial distribution of temperature distribution as a function of time (Suleman and Riaz, 2020).

Table 1.

Various parameters affecting the heating efficacy of MNPs for MNP hyperthermia

Parameters	Contributions	Characteristics	References
Types of MNP materials	Iron-oxide based MNPs (Fe_3O_4 or γ-Fe2O3 with size ranging from 10 to 100 nm)	Biocompatibility, capability of heat generation, tunable properties.	(Abenojar et al., 2016; Chang et al., 2018)
	Nanocomposite of iron oxide and metallic MNPs (e.g. Cobalt-iron oxide MNPs)	Improved heating efficacy	(Kappiyoor et al., 2010)
	Coating of iron oxide MNPs with Low Curie Temperature materials	Capability of tuning heat generation by LCT material.	(Tang et al., 2017)
Particle size	MNPs with size of 10–20 nm	Maximal heat dissipation associated with the balance between Brownian and Neel relaxations losses	(Bakoglidis et al., 2012, Engelmann et al., 2019, Purushotham and Ramanujan, 2010)
Anisotropy	Proposed an analytical model that calculates SLP values as a function of MNP anisotropy	Increase in heating power of MNP with low anisotropy	(Carrey et al., 2011)
Viscosity	Effects of supporting medium on SLP	Higher SLP values in water than viscous glycerol	(Kalambur et al., 2005)
		Lower SLP values in cellular environment	(Di Corato et al., 2014)
Field strength and Frequency of AMF	Effects of field strength (H) and frequency (f) of AMF on SLP	SLP varies linearly with f and H^2	(Cervadoro et al., 2013)
		Non-specific heating becomes negligible at f<1MHz	
	Threshold of the product of H and f for humans	$H \times f = 5 \times 10^8$ A/m·s - 8.5×10^8 A/m·s	(Johannsen et al., 2007; Maier-Hauff et al., 2007)
MNP concentration	Applied a numerical method to determine MNP concentrations for therapeutic efficacy	Estimated an optimal concentration of MNP that achieves sufficient heating for a brain tumor model.	(Bellizzi et al., 2016)
MNP Distribution	A bio-heat model with 3D lattice Boltzmann method to estimate the effect of MNP dispersion on temperature elevation	Enhanced heat dissipation for MNPs dispersed by Gaussian distribution over homogenously dispersed MNPs	(Golneshan and Lahonian, 2011)
	Clustered MNPs	Attenuation of heating efficiency and SLP values due to decreases the cluster domain magnetization and the average magnetic moment	(Wang et al., 2017)

Table 2.

Advantages and limitations for different bio-heat models

Type of Models	Advantages	Limitations
PBHTM	Inclusion of blood perfusion and metabolic heat effects (Pennes, 1948)	The classical Fourier's law which assumes that the velocity of thermal wave propagation is not valid for inhomogeneous biological tissue
	Easy to implement (Shih et al., 2007)	(Ahmadikia et al., 2012)
	Analytical solution is possible (Shih et al., 2007)	Difficult to apply complex boundaries (Kumar et al., 2016) and geometries (Lahonian and Golneshan, 2011)
		Complexity in analytical analysis for robust problem (Lahonian and Golneshan, 2011).
TWBHTM	Overcome the shortcoming of PBHTM by accounting for the delay effect of the local heat influx (Cattaneo, 1958).	Not easy to implement (Cattaneo, 1958).
	Microscale response in time domain (Cattaneo, 1958)	Limitation in describing heat transfer process occurring in space domain (Kumar et al., 2015)
	Non-Fourier effect (Ahmadikia et al., 2012)	Mathematical difficulties in dealing with the boundary conditions at the interface layers of tissue (Kuo-Chi et al., 2011)
DPLBHTM	Enables more accurate prediction of temperature distribution by incorporating the relaxation behavior of both the heat flux and temperature gradient (Tzou, 1997)	Complexities in time-phase measurement (Cattaneo, 1958).
	Captures the microscale responses in both time and space (Kumar et al., 2015)	Mathematical difficulties in dealing with the boundary conditions at the interface layers of tissue (Kuo-Chi et al., 2011

Table 3.

Applications of different bio-heat models and solving techniques for tumor tissue models

Applications	Modeling types	Solving techniques	References
Brain tumor	PBHTM coupled with Maxwell's model	SEMCAD X software.	(Bellizzi et al., 2016)
	PBHTM	Zubal numerical phantom.	(Rast and Harrison, 2010)
Liver tumor	PBHTM	Fourier series solution in polar coordinates	(Attar et al., 2014)
	PBHTM combined with Maxwell Model	Thermo-viscoelastic behavior of tumorous and healthy bovine liver tissue using a Finite difference method	(Attar et al., 2016)
	PBHTM combined with Arrhenius Kinetic Model	Finite element method using COMSOL Multiphysics	(Suleman and Riaz, 2020)
Breast tumor	PBHTM	Phantom based numerical method.	(Miaskowski and Sawicki, 2013)
	Modified PBHTM with Robin's Boundaries	Phantom based computer model.	(Miaskowski and Subramanian, 2019)
Cell death prediction	PBHTM with improved Arrhenius kinetic model	Coupled numerical model.	(Pearce et al., 2017)
	PBHTM	FEM using SEMCAD X software.	(Subramanian et al., 2016)